Available online at www.sciencedirect.com
ScienceDirect
Journal of Power Sources 177 (2008) 595–609
JOURNAL OF POWER SOURCES
www.elsevier.com/locate/jpowsour

Review

Thermal activated ("thermal") battery technology Part IIIa: FeS_2 cathode material

Patrick J. Masset [a,*], Ronald A. Guidotti [b]

[a] *Karl Winnacker Institut der Dechema e.V., Theodor-Heuss-Allee 25, 60486 Frankfurt am Main, Germany*
[b] *Sierra Nevada Consulting, 1536, W. High Pointe Ct., Minden, NV 89423, USA*

Received 13 July 2007; received in revised form 1 November 2007; accepted 1 November 2007
Available online 17 November 2007

Abstract

This article presents an overview of the pyrite FeS_2 used as cathode material in thermally activated ("thermal") batteries. A large emphasis was placed on the physicochemical properties and electrochemical performance of the pyrite FeS_2, including the discharge mechanisms, self-discharge phenomena, and recent developments.

Keywords: Thermal batteries; Molten salts; Cathode materials; FeS_2

Contents

* Corresponding author. Tel.: +49 697 564 362; fax: +49 697 564 388.
E-mail address: masset@dechema.de (P.J. Masset).

0378-7753/$ – see front matter © 2007 Elsevier B.V. All rights reserved.
doi:10.1016/j.jpowsour.2007.11.017

1. Introduction

Thermally activated ("thermal") batteries are mainly used for military purposes that require a high level of reliability and whose performance is not compromised after lengthy storage times. Applications and the electrochemistry of such power sources were described in detail in the first part of this review dedicated to thermal batteries [1]. The properties of molten salts (high- and low-temperature electrolytes) were thoroughly reviewed in the second part of this review [2]. The third part of this review of thermal batteries is devoted to the cathode materials. Thermal batteries are complex chemical systems that include electrochemical, chemical and physical properties that should be well mastered to understand the global functioning of these systems. To reach the high level of confidence required by such electrical generators, the physicochemical properties of the cathode materials must be well assessed and understood. The main physicochemical properties required for the cathode materials to be used in thermal batteries are highlighted below:

- Redox potential: it should have a discharge potential compatible with the electrochemical window of the electrolyte in order to avoid its oxidation.
- Ability to provide a fixed discharge plateau: it should undergo multiphase discharge and not intercalation.
- High thermal stability: to minimize thermal decomposition and associated possible chemical reactions caused by the decomposition products (e.g., S_2 in the case of FeS_2 reacting with the anode or pyrotechnic source in the battery). These products can also results in increased self-discharge.
- Electronically conductive: to minimize the resistance of the cathode.
- Low solubility of the cathode materials in the molten electrolyte: to minimize self-discharge reactions with attendant loss in capacity.
- Low solubility of discharge products in the molten electrolyte: to minimize possible self-discharge reactions.
- Stable towards moisture and/or oxygen: to prevent the production of oxides at the cathode surface. (This gives rise to a voltage peak at the beginning of discharge.)
- Ability to be wetted by electrolyte: to minimize the contact resistance at the electrolyte (separator)/electrode interface.
- Low equivalent weigh: for higher coulombs/mole.
- Good discharge kinetics (high exchange-current density): for high-rate capability.
- Reasonable costs.
- Being environmentally friendly ("green") is an additional desirable attribute.

This review on cathode materials is shared in two parts: this first one is dedicated to the pyrite FeS_2 and the second part concerns the other sulfides and oxide-based cathodes [160]. In this paper, the properties and performances of pyrite material are reviewed. Its properties were analyzed with regard to their use as cathode material in thermal batteries. The most important properties for thermal-battery applications are highlighted.

2. Physicochemical properties

The use of pyrite as a cathode in high-temperature batteries was first reported in a patent by Schneider and Bowser in 1978 [3]. In the beginning of the 1980s, the FeS_2 cathode was extensively studied by Argonne National Laboratory (ANL) for rechargeable applications [4] for replacement of FeS. At

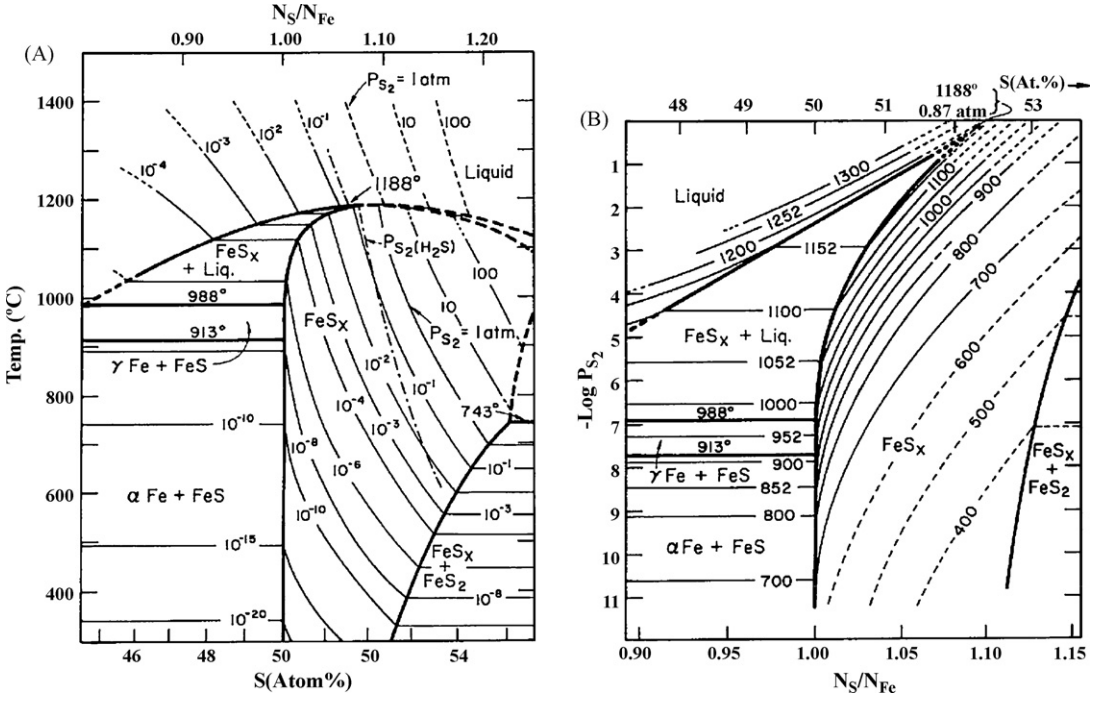

Fig. 1. Fe–S phase diagram (from Ref. [6]).

Table 1
Selected values of the thermodynamic properties of FeS and FeS_2 [26]

T (K)	ΔH_f° (kJ mol^{-1})	S_f° (J K^{-1} mol^{-1})	$C_p(T)$ (J K^{-1} mol^{-1})	ΔH_t (kJ mol^{-1})
FeS				
298	−100	60.29	$-0.5 + 170.71 \times 10^{-3} T$ (K)	–
411	–	–	72.8	2.4
598	–	–	$51.04 + 9.96 \times 10^{-3} T$ (K)	0.5
1461	–	–	50.54	32.3
FeS_2				
298	−178.2	52.93	$68.95 + 14.1 \times 10^{-3} T$ (K)–$9.87 \times 10^5/T^2$ (K)	

that time, pyrite was the most widely used cathode material in thermal batteries. Therefore the properties and performances of pyrite are covered in greater detail here.

2.1. Basic properties

The thermodynamic properties of FeS_2 are well established. FeS_2 exists in two forms: pyrite and marcasite. Pyrite is the stabile phase of FeS_2 above 700 K (see the Fe–S phase diagram in Fig. 1). The Fe–S phase diagram has been widely investigated [5,6] and recently optimized [7]. FeS_2 has a cubic structure (group P_{a3} (T_h^6)) where the Fe atoms and S_2 groups are located on the Cl and Na positions in the NaCl-type structure, respectively. The atomic positions in the cubic structure are (u is close to 0.386):

Fe: 0 0 0; 0 1/2 1/2; 1/2 0 1/2; 1/2 1/2 0
S: +/− (u u u; $u + 1/2$, $1/2 - u$, $-u$; $-u$, u, $u + 1/2$; $1/2 - u$, $-u$, $u + 1/2$)

The pyrite can deviate from the ideal stoichiometry of 2.00 by as much as 7.5 at.% but this does not greatly affect either the lattice perfection or the cube edge of the material [8].

The basic properties of FeS_2 vary with the ore's origins. The bonding in pyrite and related chalcogenides has been the subject of numerous investigations [9–13]. The band structure of the pyrite was determined by Ennaoui et al. [14]. Pyrite is a good semiconductor – both n and p types being reported – with electrical conductivities at room temperature ranging from 0.03 to 333 S cm^{-1} [15–18]. Energy gaps range from 0.77 to 1.2 eV (1.2 eV [19], 1.14 eV [15], 1.0 eV [20], 0.92 eV [21,22], 0.92 eV [23] at 300 K and 0.77 eV [24] at 550 K). It was shown that the energy gap decreases with temperature [25] which enhances the metallic character of the pyrite. This makes it perfect for use in thermal batteries, as it has a higher electrical conductivity at elevated temperatures.

Selected values of the thermodynamic properties of FeS and FeS_2 from Kubaschewski et al. [26] are reported in Table 1. The heat capacity of FeS_2 was measured [27–29] and recently re-investigated [30]. However, some discrepancies appeared. The latter is approximately 10% higher in the temperature range investigated (Fig. 2). The heat of vaporization of FeS_2 ΔH_{vap} has been measured by several techniques. ΔH_{vap} values as well as the techniques used are reported in Table 2. From literature data [31–42] the decomposition temperature T_d is given by Eq. (1).

$$T_d\,(^\circ\mathrm{C}) = \frac{15,700}{[16.2 - \log P_{vap}]} - 273 \quad (1)$$

where P_{vap} represents the sum of the partial pressures of the sulfur-based species S_n. The decomposition temperature is lowered in presence of impurities in pyrite ores [43].

2.2. Stability

2.2.1. Oxidation

Sulfates form rather easily on the pyrite surface even at low oxygen pressure as sketches the predominance diagram shows (Fig. 3). In nature, topochemical pyrite oxidation to $FeSO_4$ occurs readily and is depends greatly on the ambient moisture content of the air, being greatly accelerated above 20% relative

Table 2
Thermodynamic data relative to pyrite and marcasite decomposition

Temperature range (°C)	ΔH_{vap}° (kJ mol^{-1} FeS_2)	Reference	Experimental technique
647–681	449	[32]	Manometry
575–680	412	[33]	Condensation temperature
590–686	383	[34]	Manometry
600–690	327	[35]	Manometry
324–743	304	[36]	
500–552	301	[37]	Manometry
436–591	297	[38]	Transpiration
324–438	292	[39]	Sensitive sensor
547–743	276	[40]	Manometry
548–676	266	[41]	Manometry
695–770	268 (marcasite to troilite)	[43]	Torsion–Knudsen effusion, transpiration
420–600	234	[42]	Isotopic tracer

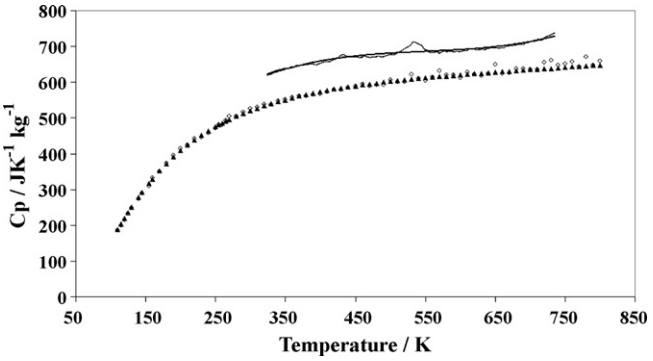

Fig. 2. Experimental values of C_p of FeS_2 versus the absolute temperature, (▲) data from Ref. [29], (◯) data from Ref. [30], (—) data from Ref. [31].

humidity [44]. Oxidation activation energy of 27.2 J mole^{-1} was reported. Surface oxidation of pyrite has been reported to be dependent on the temperature and humidity as well as the particle size [45]. Experimentally, sulfate crystal growth has been evidenced by XPS measurements on fresh pyrite surface in vacuum [46]. The thermal decomposition of sulfates leads to the formation of Fe_2O_3 [47,48]. A large voltage transient ("spike") occurs upon activation of a thermal battery if the FeS_2 contains impurities such as oxides, sulfates, and elemental sulfur or if the activity of Li is not fixed in the cathode. This interferes with maintaining strict voltage control. This is readily remedied by lithiation, however [49–52]. Common lithiation agents are Li_2O or Li_2S, added in small quantities of 1–2 (w/o). It should be mentioned that pure S was also tested as anti-peak agent [53]. The starting pyrite used in the cathode is leached with a 1:1 (v/v) solution of HCl to remove the major portion of the impurities, leaving behind siliceous gangue, which is electrochemically inert. This gangue can also be removed by leaching with concentrated HF, if a higher purity pyrite is desired or required. An alternative, mineral beneficiation technique, such as flotation, can also be used for pyrite purification [54].

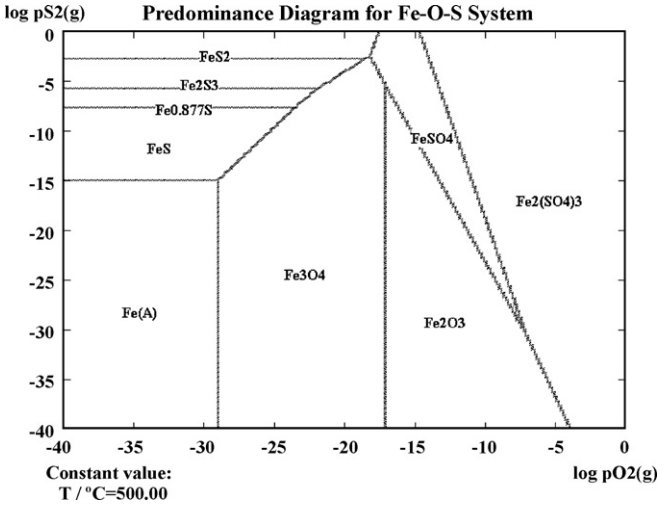

Fig. 3. Predominance diagram of the Fe–S–O system at 500 °C.

2.2.2. *Thermal stability in inert atmosphere*

The thermal stability of pyrite has been widely investigated under inert or corrosive atmosphere by non-isothermal or isothermal analyses [46,55–69,37]. The overall mechanism is described by Eq. (2).

$$(1-x)FeS_{2(s)} \rightarrow Fe_{1-x}S_{(s)}\,(x = 0\text{–}0.2) + \tfrac{1}{2}(1-2x)S_{2(g)} \quad (2)$$

By isothermal analysis it was shown that the mass losses during the decomposition process were linear with time. In addition, the dependence of the kinetic constant versus temperature follows an Arrhenius-type law [68]. The activation energy varied between 275 and 325 kJ mol^{-1} FeS_2. Literature values of the activation energy and experimental conditions are reported in Table 3. Values of the activation energy determined either by non-isothermal or by isothermal analysis were found to be similar [68]. During its thermal decomposition, the pyrite is progressively transformed into pyrrhotite and the FeS_2 grains

Table 3
Kinetics data relative to pyrite decomposition

Temperature range (°C)	Activation energy (kJ mol^{-1})	Reference	Experimental conditions
500–600	230	[46]	Linear weight loss, isothermal analysis, dry He flow—50 cm^3 min^{-1}
500–600	260	[46]	Linear weight loss, isothermal analysis, dry He flow—50 cm^3 min^{-1}
400–750	110	[55]	Linear weight loss, isothermal analysis, vacuum and Ar atmosphere
450–690	110	[56]	Linear weight loss, isothermal analysis, vacuum and N_2 atmosphere
486–554	120	[57]	Linear weight loss, isothermal analysis, vacuum
400–650	130	[58]	Linear weight loss, isothermal analysis, air, CO_2 and H_2 atmosphere
390–530	140	[59]	Linear weight loss, isothermal analysis, air, CO_2 and mixtures
400–550	297 ± 34	[37]	Linear weight loss, isothermal analysis, dry He and N_2 flow 100 cm^3 min^{-1}
450–600	297 ± 15	[37]	Linear weight loss, isothermal analysis flow (with 54, 108 and 1003 ppm CO)
450–600	275 ± 20	[37]	Linear weight loss, isothermal analysis, CO_2 atmosphere
T<475	82 ± 9	[37]	Linear weight loss, isothermal analysis, flow with 100 ppmv O_2
T>475	293 ± 52		
600–653	281	[60]	Linear weight loss, isothermal analysis, Ar atmosphere
427–927	286	[61]	Linear weight loss, isothermal analysis, N_2 atmosphere
451–476	310	[62]	Linear weight loss, isothermal analysis, vacuum
594–625	–	[63]	Fluidized bed, linear variation of the S/Fe ratio with time
620–643	–	[64]	Fluidized bed, linear variation of the S/Fe ratio with time
610–750	–	[65,66]	Fluidized bed, linear variation of the S/Fe ratio with time
25–800	325	[67]	First order-based analysis, non-isothermal analysis (v = 10 °C min^{-1})

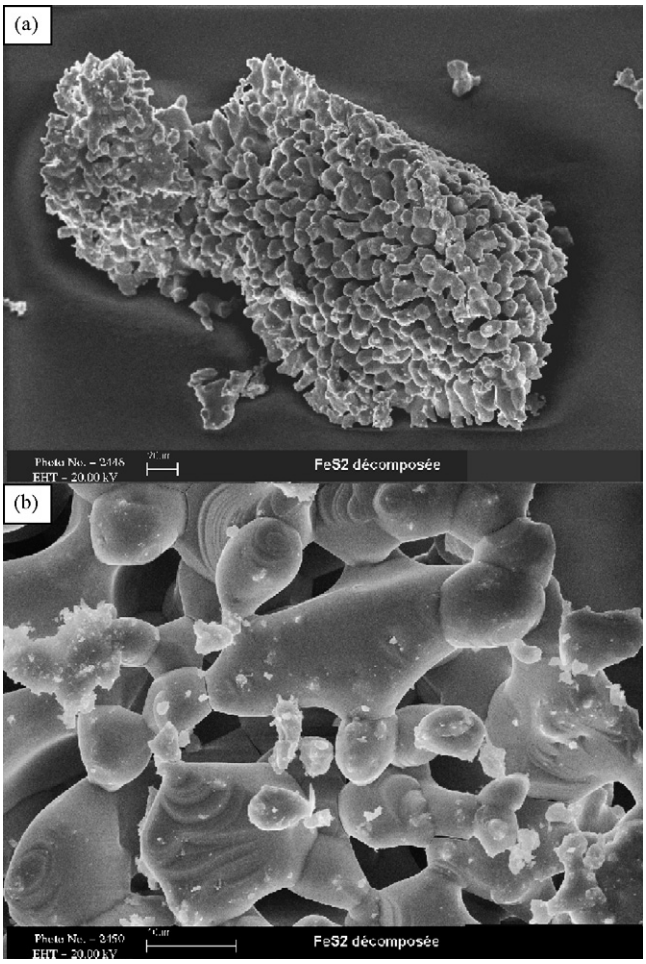

Fig. 4. SEM picture of decomposed FeS_2 (a) grain and (b) detail.

become porous as sulfur gas escapes (Fig. 4). The mechanism of FeS_2 and $FeS_{1.14}$ thermal decomposition was investigated and modelled by Hoare [61]. When synthetic pyrite is compared to natural pyrite, thermal decomposition occurs more slowly for equivalent grain size [46]. This was attributed to the lower intrinsic purity of the mineral material.

In contrast to pyrite, the thermal decomposition of FeS (troilite) does not become significant until 1200 K, being only ~0.47 kPa [42]. The vapor pressure of sulfur over troilite is given by Eq. (3):

$$\ln pS_2\,(\text{kPa}) = 8.03 - \frac{16,040}{T}\,(\text{K}) \tag{3}$$

2.2.3. Thermal stability in molten salts

Above 580 °C FeS_2 thermally decomposes to form a non-stoichiometric monosulfide (pyrrhotite) and sulfur vapor which reacts exothermic ally with the lithium or lithium-alloy anode or dissolved lithium in the molten electrolyte. It can also react with the hot iron in the pyrotechnic used in the battery. This reduces the battery capacity as well as generating more heat. This, in turn, leads to even more thermal decomposition of FeS_2, which can then destroy the battery if thermal runaway occurs. Moreover, it forms solid insulating Li_2S layer in the retained electrolyte [70].

Table 4
Expression of the solubilities of sulfur-containing species (Li_2S, FeS_2, $FeS_{1.14}$) versus the temperature in the LiCl–KCl eutectic

	$\ln XM_xS_y$ (10^{-4} mole fractions)	Reference
Li_2S	$11.077 - 6.1046 \times 10^3/T$ (K)	[72–77]
FeS_2	$10.753 - 11.882 \times 10^3/T$ (K)	[71]
$FeS_{1.14}$	$6.4477 - 7.6622 \times 10^3/T$ (K)	[71]

The pyrite as well as the pyrrhotite dissolves partially in molten salts at high temperature. Solubility limits of FeS_2 [71], $FeS_{1.14}$ [71] and Li_2S [72–77] were experimentally measured. Analytical expressions of the solubility limits of FeS_2, $FeS_{1.14}$ and Li_2S in the LiCl–KCl eutectic are reported in Table 4. In Fig. 5, one can observed that at high temperature the solubility limits of FeS_2 and $FeS_{1.14}$ were equal which agrees the progressive decomposition of FeS_2 into $FeS_{1.14}$ at high temperature. Santarini [78] established the FeS_2–pS_2-predominance diagram in the LiCl–KCl eutectic. It was found that the solubility limit of Li_2S was lower than in other studies. It was ascribed to the formation of the so-called J-phase that forms between FeS_2 and the LiCl–KCl eutectic above 470 °C [4,79]. The J-phase has the djerfisherite structure and the general composition $K_{5.5}Li_{0.6}Fe_{24}S_{25.9}Cl_{1.0}$ [80,81] (Fig. 6).

As the pyrite thermally decomposes, sulfur gas is able to react with already dissolved sulfur-based species [82] according the following mechanism to form polysulfides [83]. Those reactions (Eq. (4)) might enhance the dissolution process. The stability of sulfur-based species in molten chlorides was studied by Delarue [84] even in presence of dissolved oxide ions [85–87].

$$\begin{aligned} 2S^{2-} + 3S_2 &\Leftrightarrow 4S_2^- \\ 2S^{2-} + 5S_2 &\Leftrightarrow 4S_3^- \end{aligned} \tag{4}$$

The decomposition kinetic of FeS_2 in molten salts has been little investigated by Barlow [88], who reported the thermal stability of pyrite in the molten LiCl–KCl and LiF–LiCl–LiBr eutectics. More recently Masset et al. measured the thermal

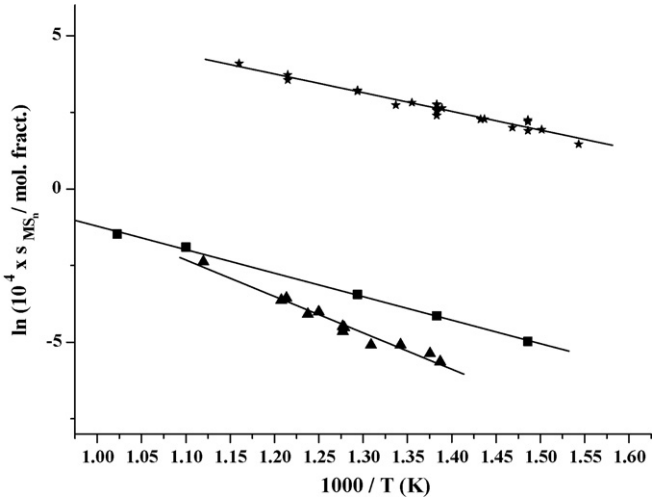

Fig. 5. Evolution of the logarithm of Li_2S, FeS_2 and $FeS_{1.14}$ solubility in the LiCl–KCl eutectic versus the inverse of the absolute temperature. (⋆) Li_2S data from Refs [72–77], (■) FeS_2 from Ref. [71], (▲) $FeS_{1.14}$ from Ref. [71].

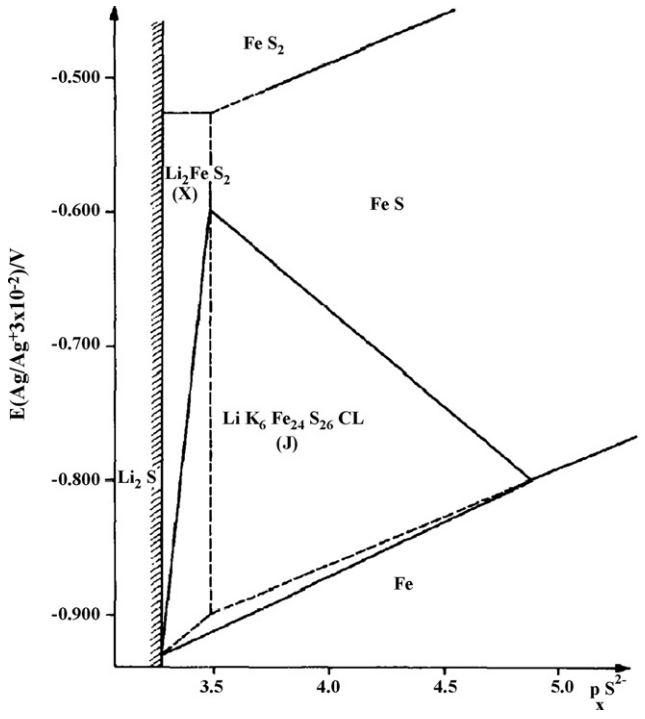

Fig. 6. FeS_2–pS_2-predominance diagram in the LiCl–KCl eutectic [79].

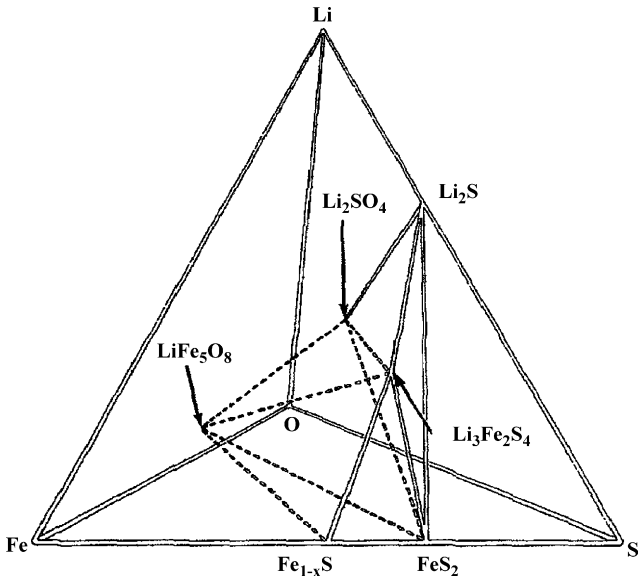

Fig. 7. Li–Fe–S–O phase diagram [51].

decomposition kinetics in LiX–KX (X = Cl, Br, I) mixtures, in the LiF–LiCl–LiI and LiF–LiCl–LiBr electrolytes [68,89]. In many cases the weight variations varied linearly with time. Moreover, a linear relationship was evidenced between the kinetic constant and the radius of the anion X^- [68]. The activation energy of the reaction was found close to 300 kJ mol^{-1} FeS_2 in LiX–KX mixtures (X = Cl, Br, I) whereas it was approximately equal to 360 kJ mol^{-1} FeS_2 in ternary mixtures. In molten media the kinetic constants are at least three orders of magnitude lower than in inert gas atmosphere. The molten salt probably acts as a physical barrier for the ready escape of the sulfur gas and may repress dissociation by increasing the partial pressure of sulfur in the immediate vicinity of the discrete FeS_2 particles.

The influence of dissolved hydroxides or oxides in the electrolyte on the chemical stability of the pyrite has been poorly investigated. The temperature of thermal decomposition of FeS_2 in the LiCl–KCl eutectic was investigated by means of thermogravimetric analysis (TGA) in the presence of hydroxides [30] and oxides [30,90]. The beginning of the thermal decomposition is a function of the amount of hydroxides or oxides contained in the electrolyte. According to the quaternary phase diagram Li–Fe–S–O (see Fig. 7) [50,91], the reaction pathway leads to the formation of $Li_3Fe_2S_4$ by adding Li_2O to the pyrite. The weight variations recorded during the TGA experiments are in good agreement with these theoretical predictions.

The wetting properties of pyrite by molten salts may also be influenced by the morphology changes during the decomposition step as the pyrite becomes more and more porous. This might also modify the interface properties between the cathode material and the electrolyte. The poor wetting behavior of the pyrite by the molten LiCl–KCl eutectic has been previously reported (wetting angle: 120° at 500 °C [30]). To our best knowledge no wetting behavior of FeS has been yet reported.

One question remains unresolved: how does the molten salt fill the empty space created by the sulfur escape and how does it influence the wetting behavior (pyrrhotite formation at the pyrite surface). No wetting angles of FeS_2 or Li_3FeS_4 have been measured in the presence of dissolved oxides or hydroxides.

2.3. Chemical stability in low-melting-point electrolytes

2.3.1. Halide electrolytes

A number of alkali halide eutectic salts have been examined for potential use with pyrite cathodes for possible use in geothermal applications [2,92–97]. These batteries would not use an internal pyrotechnic but would depend on the immediate borehole thermal environment to provide the needed energy for melting of the electrolyte to allow the batteries to function. Thermal batteries typically operate over a temperature range of 400–550 °C for standard electrolytes. In contrast, borehole temperatures can be as low as 300–400 °C. In the case of boreholes associated with oil and gas drilling, the maximum temperatures are much lower—typically, only up to 250 °C. This would require the use of electrolytes that are even lower melting.

2.3.2. Nitrate electrolytes

There are a number of low-melting electrolytes based on alkali nitrates that have been examined for use in high-temperature batteries [98]. However, molten nitrates are incompatible with sulfide cathodes, oxidizing them to oxides or sulfates, with the generation of NO_x and SO_2 and considerable heat [99].

2.3.3. Organic electrolytes

A number of organic electrolytes have been examined for use with sulfide cathodes for various battery applications. For organic solvents or low-melting-point electrolytes,

the thermal stability should be replaced by the chemical stability, as the pyrite is stable in the temperature range of interest of these solvents. FeS_2 has been successfully used in room-temperature primary batteries using organic solvents (EC-PC-DME) [100–104]. Similar work with 1 M $LiClO_4$ in PC-DME and synthetic pyrite was reported by Iwakura et al. [105]. The performance of synthetic and natural pyrite in non-aqueous systems has also been studied [106,107]. The rate capabilities of the synthetic pyrite were greater than those of natural pyrite because of the finer grain size of the former. Recently, Choi et al. [108] reported the use of FeS_2 pyrite as cathode material in Li/FeS_2 temperature batteries using lithium-based salts (LiTFSI) dissolved in organic solvents as electrolyte. (Similar cells are commercially available from Eveready [109].) Considerable work has also been done with pyrite cathodes in conjunction with polymer-based electrolytes [100–104].

The use of ionic liquids – the so-called room-temperature molten salts – has also been explored as one low-temperature medium for use with the Li–Si/FeS_2 couple. This type of electrolyte has an intrinsic high-temperature stability that would allow its use for certain borehole applications. Being liquid at room temperature would allow its use from ambient to the temperatures in the borehole. While it is compatible with the cathode, such material are not compatible with high-activity anodes such as Li–Si, Li–Al, Ca, or Mg at temperatures above 100 °C [110].

More recently, another category of electrolyte has been examined, the tetraalkyl ammonium salts. The tetraalkylammonium salts have good thermal stability and a high voltage-stability window. One such salt, tetramethylammonium bis(trifluoromethylsulfonyl)imide (TMAIm) has been studied with the Li–Si/FeS_2 couple [111]. While it did function as expected, it suffered from one major problem: a very low ionic conductivity – only 85 mS cm^{-1} at 250 °C, which is more than an order of magnitude less than some of the traditional thermal-battery electrolytes – which resulted in unacceptable polarization losses. This greatly limits its possible use.

2.4. Electrochemical behavior

2.4.1. Discharge mechanism

The discharge reactions that occur when a FeS_2 cathode is used in high-temperature batteries have been extensively studied by ANL for rechargeable applications. A number of other researchers had studied the various electrode processes associated with pyrite but there was some disagreement as to the exact nature of the sequence of discharge phases in molten salts [112,113]. Schmidt, for example, postulated the formation of an "Li_2S_2" metastable intermediate [114,115]. However, the multi-step discharge mechanism put forth by ANL is felt to be the most accepted [4,116,117]. The four discharge sequences of FeS_2 in molten LiCl–KCl are described in Eqs. (5)–(8):

Step 1:

$$FeS_2 + \tfrac{3}{2}Li^+ + \tfrac{3}{2}e^- \rightarrow \tfrac{1}{2}Li_3Fe_2S_4\ (\text{"Z-phase"}) \quad (5)$$

The first discharge step consists in the reaction of 1.5 mole of lithium with one mole of pyrite. This reaction contrasts to the intercalation process, where electrochemical insertion of the lithium cation in carbon occurs (Graphite Intercalation Compounds: GIC [118]). It presents the advantage that it ensures a flat discharge plateau before the potential transition [119]. This transition is equivalent to 1206 A s g^{-1} of FeS_2.

It should be mentioned that Ritchie [120] took advantage of this reaction to produce the cathode material $Li_3Fe_2S_4$ using the spontaneous reaction of pyrite with pure LiCl and LiBr used as solvent.

Step 2:

$$(1-x)\,Li_3Fe_2S_4 \Leftrightarrow (1-2x)\,Li_{2-x}Fe_{1-x}S_2 + Fe_{1-x}S \quad (6a)$$

In Eq. (6a), x is close to 0.2.

When $x = 0$, Eq. 6b results for the reduction of $Li_3Fe_2S_4$.

$$Li_3Fe_2S_4 + Li^+ + e^- \rightarrow Li_2FeS_2 + FeS + Li_2S \quad (6b)$$

Step 3:

$$Li_{2-x}Fe_{1-x}S_2 \rightarrow Li_2FeS_2\ (\text{"X-phase"}) \quad (7)$$

Step 4:

$$Li_2FeS_2 + 2e^- \rightarrow Li_2S + Fe + S^{2-} \quad (8)$$

Li–Si[1]/FeS_2 thermal batteries are designed to use only the first cathode transition (Eq. 5) because of rigid voltage requirements associated with the use of such batteries.

The species actually undergoing reduction in Eq. (5) is the polysulfide, $S_2{}^{-2}$, i.e., the oxidation state of Fe in FeS_2 is +2 and not +4 [21,22]. This is illustrated in Eq. (9):

$$S_2{}^{-2} + 2\,e^- \rightarrow 2\,S^{-2} \quad (9)$$

FeS_2 begins to thermally decompose at temperatures above 550 °C to form a non-stoichiometric monosulfide (pyrrhotite) and sulfur vapor, as shown in Eq. (2):

Any fugitive sulfur can react very exothermically with the Li-alloy anodes in the battery. This reduces the battery capacity as well as generating more heat. This, in turn, leads to even more thermal decomposition of FeS_2, which can destroy the battery if thermal runaway occurs.

The open-circuit potentials for a number of the major discharge reactions are summarized in Table 5. Note that the first two discharge steps experience entropy changes that result in cell cooling, while the discharge of the Li_2FeS_2 phase results in cell heating [121]. These changes are very important for proper thermal management of high-temperature rechargeable batteries.

The electrolyte used in pyrite-based cells can impact the discharge processes in a number of ways. High levels of K^+ can lead to increased formation of the J-phase material

[1] All reference to Li–Si in this paper is for the composition 44 (w/o) Li/56 (w/o) Si.

Table 5
Open-circuit potentials for several of the discharge steps involving pyrite at 400 °C (from Ref. [116])

Discharge reaction	emf at 400 °C versus Li–Al (V)	Entropy effects
$FeS_2 \rightarrow Li_3Fe_2S_4$	1.750	Cooling
$Li_3Fe_2S_4 \rightarrow Li_{2+x}Fe_{1-x}S_2 + Fe_{1-y}S$	1.645	Cooling
$Li_2FeS_2 \rightarrow Fe + Li_2S$	1.261	Heating [121]

($K_{5.5}Li_{0.6}Fe_{24}S_{25.9}Cl_{1.0}$). However, this phase appears not to be stable above 500 °C. The generation of a large Li^+ flux at the anode–separator interface under high-rate discharge can lead to very high concentration gradients, with the associated localized increase in melting point of the electrolyte. This is illustrated in Fig. 8 (from Ref. [122]) for a Li–Si/LiCl–KCl/FeS_2 cell. The increase in Li^+ concentration at the anode is accompanied by a corresponding increase in the K^+ concentration at the cathode. The precipitation of solids reduces the volume of free electrolyte and increases the resistance of the separator, leading to a substantial increase in the overall impedance of the battery. This is most important near the end of life of the battery when its temperature is lowest.

The conductivity of the discharge phases also influences the performance of the cell. While the conductivity of the pyrite phase is very good, that of the first discharge phase, $Li_3Fe_2S_4$, is much lower, while that of subsequent discharge phase is intermediate. Data taken from Ref. [123] for temperatures of 400 and 500 °C are presented in Table 6. Both the starting and discharge

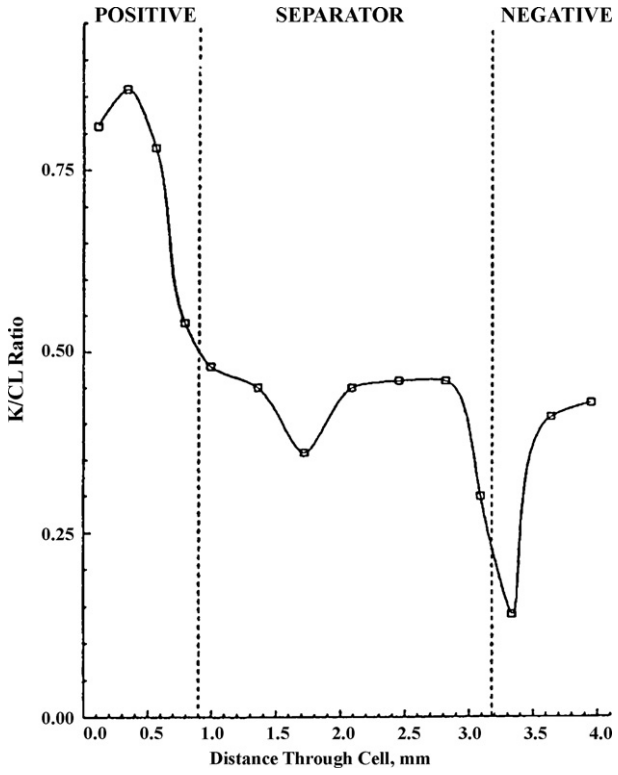

Fig. 8. Variation in atomic K/Cl ratio in Li–Si/LiCl–KCl/FeS_2 single cell discharged at 500 °C and 50 mA cm^{-2} [122]. (The nominal K/Cl ratio is 0.418 for the eutectic composition.)

Table 6
Electrical conductivities of the phases associated with the discharge of pyrite cathodes

Phase	Temperature (°C)	Conductivity (S cm^{-1})
FeS_2	400	80–100 [4,25]
$Li_3Fe_2S_4$ (Z-phase)	400	~0.1 [123]
Li_2FeS_2 (X-phase)	400	4.2 [123]
FeS_2	500	80–100 [14,26]
$Li_3Fe_2S_4$ (Z-phase)	500	~0.3 (extrapolated) [123]
Li_2FeS_2 (X-phase)	500	~6.3 [123]

phases are semiconductors, which is ideal for thermal-battery applications.

The effects of the conductivity changes in the cathode are readily apparent with the use of a suitable reversible reference electrode. For short-time runs, an Ag/AgCl (0.1 M) reference contained in a glass capillary tube sealed at one end works quite well [124]. However, after several hours, the reference deteriorates and emf becomes unstable. An aluminum wire can be charged with Li to form a two-phase region consisting of α-Al + β-LiAl. This provides a very stable emf with long discharge times. ANL developed a Ni/Ni_3S_2 reference that works very well for this purpose [125–127]. The area-specific impedances of typical anode and cathode for a Li–Si/LiCl–KCl/FeS_2 cell discharged at 450 °C and 50 mA cm^{-2} are shown in Fig. 9. As can readily be seen, the change in the anode impedance is insignificant with depth of discharge, while there is a dramatic increase for the cathode. This is similar to what was reported by Wang [128]. Using rotating disc voltammetry, he found that the bulk of the total cell polarization (~75%) is associated with the porous cathode. The bulk of the observed increase in impedance is due to the formation of the less-conductive Z-phase at the start of discharge. There is some contribution as well from KCl precipitation (see Fig. 8) and J-phase formation. At normal discharge rates associated with thermal batteries, the Z-phase begins to discharge to form the X-phase before all of the

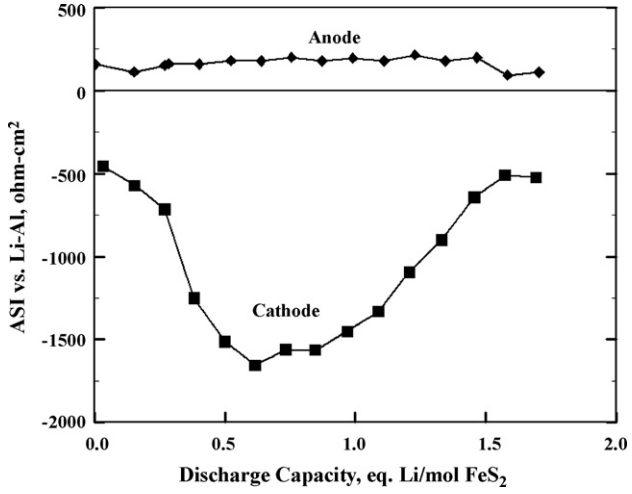

Fig. 9. Area-specific impedances of half cells of a Li–Si (25% electrolyte)/LiCl–KCl/FeS_2 cell discharged at 450 °C and 50 mA cm^{-2} [122].

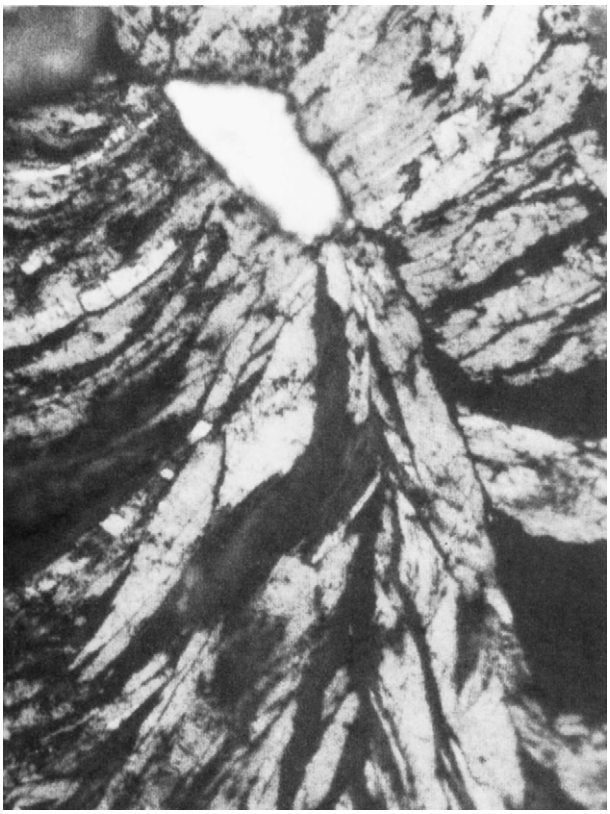

Fig. 10. Photomicrograph of FeS_2 phase (white) and $Li_3Fe_2S_4$ phase (light gray) (650×) formed during discharge of Li–Si/LiCl–KCl/FeS_2 cell at 400 °C and 50 mA cm^{-2} [122].

initial pyrite phase is consumed. The discrete discharge phases are readily evident in the photomicrograph of Fig. 10. There is a large volumetric change in the cathode during discharge due to the lower density of the Z-phase. This can lead to mechanical issues for secondary high-temperature batteries using pyrite cathodes.

2.4.2. Ambient temperature applications

When FeS_2 is discharged at temperatures of 200 °C or more, the reaction is quite reversible. However, when Li/FeS_2 cells are discharged at ambient temperatures using organic electrolytes, the discharge reaction is not completely reversible. The Z-phase which is the first discharge product of pyrite cathodes in molten salts does not form in nonaqueous systems. Instead, the X-phase is observed [109,105]. The reversibility in nonaqueous systems was also studied by Fong et al. [129,130].

2.4.3. Self-discharge

The decrease in battery efficiency comes mainly from self-discharge reactions. In this system where complex electrochemical and chemical reactions take place, the knowledge and the understanding of the source of these unwanted self-discharge reactions are of great importance. Both the pyrite and Li–Si have finite solubilities in the molten salts. (In the case of pure Li, a solubility of 0.038 mol l^{-1} has been reported in LiCl–KCl eutectic at 400 °C [2].) This leads to the creating of a flux of migrating dissolved species, such as Fe^{+2}, polysulfides,

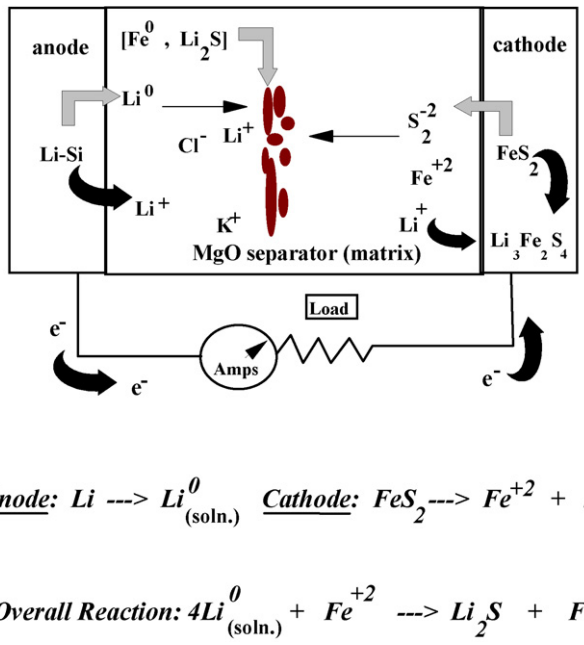

Fig. 11. Schematic representation of self-discharge reactions in Li–Si/LiCl–KCl/FeS_2 cells.

and elemental Li. Wang and Seefurth also hypothesized the presence of dissolved Fe compounds in the electrolyte that resulted in loss of capacity of similar cells [113]. The discharge mechanism is illustrated schematically in Fig. 11. The reacting solution species migrate towards each other and react in the separator matrix. The band of reaction product appears orange colored under polarized light. (However, when Li_2FeS_2 is substituted for FeS_2, no band formation is observed [122] because of the reduced solubility of this FeS-containing phase.) The rate of self-discharge is very dependent upon temperature, Li activity of the anode, and electrolyte composition [131]. Data for the LiCl–KCl eutectic electrolyte are presented in Table 7 [132]. These data are in agreement with a study by Burrow et al. where discharged Li–Si/FeS_2 cells were cross-sectioned and the anode–separator and cathode–separator interfaces were examined by scanning electron microscopy (SEM), energy dispersive X-ray analysis (EDX), and Auger electron spectroscopy (AES) for elemental distribution [133].

This proposed discharge mechanism is supported by the identification of elemental Fe and Li_2S crystals in the center of the separator of discharged Li–Si/FeS_2 cells [122,134,70]. The amount of Li_2S that forms is found to be related to the activity of the anode used, with high activity (e.g., pure Li) associated with greater levels of Li_2S deposition. The Li_2S level also increases with increase in the Li^+ content of the electrolyte. The reaction

Table 7
Rate of self-discharge for pure Li in LiCl–KCl eutectic electrolyte [132]

Temperature (°C)	Self-discharge rate (mA cm^{-2})
395	1.0
415	1.4
436	1.9

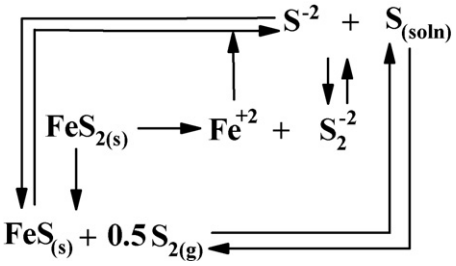

Fig. 12. Equilibria among various species for FeS_2 in contact with molten electrolyte.

band tends to move closer to the cathode with increasing Li activity of the anode [70].

The equilibria between the various species in the case of pyrite in contact with molten electrolyte are summarized in Fig. 12. There is competition between decomposition of FeS_2 to FeS and sulfur gas, which can dissolve in the electrolyte. In addition, the polysulfide will be in equilibrium with sulfide and dissolved sulfur. Once the solubility limit of FeS is reached, it can precipitate out of solution. The relative importance of these associated reactions is not known at this time. In the presence of significant K^+ concentrations, formation of the J-phase can also occur at temperatures above 470 °C.

The composition of the electrolyte has a major influence on the solubility of pyrite and self-discharge of Li–Si/FeS_2 cells (Table 8). The concentration of Li^+ appears to be responsible for this behavior. With a K-rich LiCl–KCl electrolyte, a discharge loss rate of 0.001% h^{-1} was reported at 450 °C and 88 mA cm^{-2} [113]. This increased to 0.013% h^{-1} for the stoichiometric composition. With a K-free electrolyte of LiCl–LiBr–LiF, the self-discharge rate increased to 0.07% h^{-1}. Dissolution of FeS_2 has also been reported even in low-melting, tetrachloroaluminate melts. Solubilities of 6.8×10^{-4} and 2.0×10^{-3} mole fractions at 170° and 270 °C, respectively, were reported [135].

Similar capacity-loss behavior has been observed at Sandia National Laboratories (SNL). Self-discharge of Li–Si/FeS_2 cells

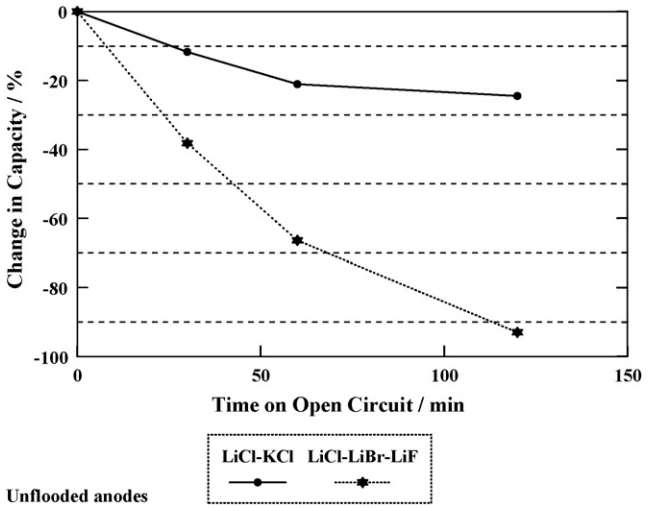

Fig. 13. Self-discharge losses for Li–Si (25% electrolyte)/FeS_2 cells at 500 °C as a function of time on open circuit prior to discharge at 125 mA cm^{-2} for LiCl–KCl and LiCl–LiBr–LiF electrolytes.

increased with increasing temperatures and with decreasing current densities, with open circuit being the worst condition [131]. Significant loss in capacity of Li–Si/FeS_2 cells was observed when the cells were place on open circuit for up to 2 h. While substantial loss was observed for the LiCl–KCl eutectic, the loss was greatest for the all-Li (K^+-free) LiCl–LiBr–LiF electrolyte. The response at 500 °C is shown in Fig. 13. In the former case, the loss in capacity was almost 12% after 30 min but did not increase much more after 2 h. For the all-Li electrolyte, however, the corresponding value was over 38%, for 30 min open circuit. After 2 h, almost all of the capacity has been exhausted (>93%). Fortunately, such conditions are not encountered during normal thermal-battery operation and are more important for secondary applications.

When FeS_2 is equilibrated with various molten halide eutectic mixtures, an amber-colored solution is formed. (Similar colored solutions were observed in the electrochemical study of sulfur

Table 8
Self-discharge rate of FeS_2 cathode (open circuit) [131]

Electrolyte	Catholyte treatment	T (°C)	Capacity losses (% min^{-1})	(r^2 for LSF)
LiCl–KCl	Fused, unlithiated	450		0.9889
		550	0.450	0.98703
	Fused, lithiated	450	0.0915	0.9942
		550	0.438	0.9997
LiBr–KBr–LiCl (LM#1)	Fused, unlithiated	450	0.130	0.9778
		550	0.582	0.9534
	Fused, lithiated	450	0.0998	0.5396
		550	0.330	0.95029
LiBr–KBr–LiF (LM#2)	Fused, unlithiated	450	0.344	0.99965
		550	0.751	0.98379
	Fused, lithiated	450	0.203	0.99467
		550	0.354	0.99467
LiCl–LiBr–LiF (all-Li)	Fused, unlithiated	450	0.374	0.98507
		550	0.722	0.97499
	Fused, lithiated	450	0.448	0.92364
		550	0.716	0.88492

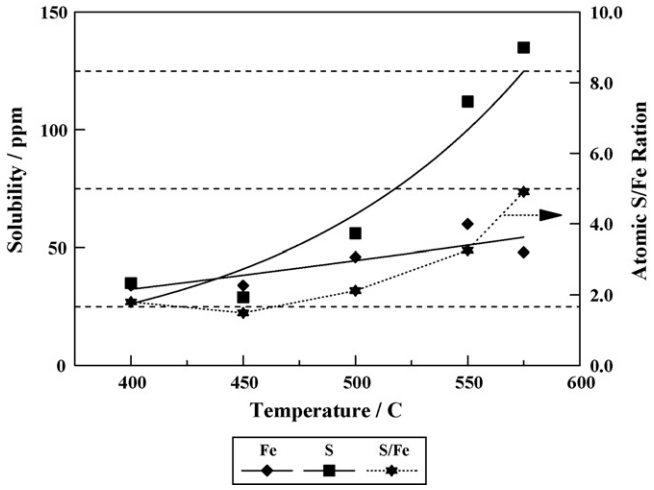

Fig. 14. Soluble S and Fe as a function of temperature for a solution of LiCl–KCl eutectic equilibrated with FeS_2 for 1 h.

and sulfide in LiCl–KCl eutectic and were attributed to complexed sulfur species [136].) Analysis for Fe and S of filtered and quenched aliquots of these solutions show that the dissolved S increases sharply with temperature. However, the soluble Fe content changes little and, in some cases, actually decreases over the same temperature interval. This is shown in Fig. 14 for the LiCl–KCl eutectic. These data indicate that Fe^{+2} is being removed by precipitation of FeS (or Li_xFeS_y species) by the reactions shown in Fig. 12. As a result, the atomic S/Fe ratio is not fixed at 2 but increases rapidly with temperature above 500 °C. Similar results were obtained with other electrolytes, with a S/Fe atomic ratio of 13 at 550 °C for the LiCl–LiBr–LiF electrolyte. The trend in solubility of FeS_2 in molten salts with temperature and electrolyte composition mirrors that observed for Li_2S. The data of Table 9 show that the solubility increases considerably with temperature with the all-Li electrolyte showing the greatest solubility [137].

These solubility data are for FeS_2 in the absence of the Li-alloy anodes. In a complete cell, the reaction of the migrating soluble Li° species with the soluble species arising from the FeS_2 will also be taking place and is reflected in the self-discharge behavior of such cells. Under moderate rate (e.g., 400–500 mA cm^{-2}) discharge, the self-discharge reactions will not generally be significant, as the electrochemical reactions will dominate the chemical reactions that can occur in parallel during discharge.

The dissolution of elemental Li from the anodes adds further complicates matters in that it gives rise to electronic conductivity in the molten salt. This has been reported for a number of alkali metal–alkali halide (M–MX) systems [138–142]. Reynolds et al. used the Wagner polarization technique to study the contribution to the electronic conductivity of LiCl–KCl electrolyte as a function of Li activity of the anode [143]. Dissolved Li can be represented by Eq. (12).

$$Li^{\circ}_{(soln)} \rightarrow Li^{+} + e^{-} \quad (12)$$

They reported an electronic conductivity of 0.18 S cm^{-1} for pure Li (unit activity) at 465 °C and 8×10^{-5} S cm^{-1} at 383 °C for $Li_{0.75}Al$ alloy (0.056 Li activity).

Table 9
Solubility of Li_2S in various molten salts [137]

Electrolyte composition (m/o)	Temperature (°C)	Li_2S solubility (ppm)
65LiCl/35KCl	400	1100
55LiCl/45KCl (eutectic)	400	650
66LiCl/34KCl	500	1800
54LiCl–46KCl	500	840
22LiF–31LiCl–47LiBr	466	6840
22LiF–31LiCl–47LiBr	500	8700

3. Recent developments

3.1. Nanostructured FeS_2

Nanostructured FeS_2 prepared by a high-energy grinding process and used as the cathode material in $LiSi/FeS_2$ thermal batteries resulted in improved electrochemical performance [144]. With the same weight, the nanostructured cathode pellets were reported to be 23% thinner than conventional counterparts resulting in 31% increase of pellet density. With the nanostructure, the electrode materials react more rapidly and completely. The nanostructured cathode pellets are more mechanically robust than the conventional materials, which leads to potential high productivity and lower cost in battery manufacturing. Only data for single-cell tests at one temperature were reported. These limited data are in agreement with more comprehensive data generated over a wide range of discharge conditions for pyrite and other disulfides synthesized by an aqueous method [145]. Using nanostructured materials, it is expected that thermal batteries can be prepared that are more compact and robust with higher energy density.

3.2. Thermal-sprayed electrode

All thermal-battery electrodes today are formed by pressing powder mixes into pellets that are then stacked to construct the battery. This requires increasing larger – and expensive – presses as the pellet diameters increase. (The forming pressure will increase as the square of the pellet diameter.) The large inventory of pressing dies that are necessary adds to the equipment costs. Several years ago, the concept of plasma spraying of thermal-battery electrodes was evaluated [146–156]. This approach involves using a thermal-spray process to deposit thin-film electrodes onto a graphite-paper or stainless steel current collector. It was demonstrated that both FeS_2 [154,156] and CoS_2 [156] cathodes could be formed in this fashion.

The main advantages of this type of cathode are:

- better mixing of the electrolyte and pyrite in the electrode layer;
- decrease of the cathode thickness (volume gain, since one can deposit only what is necessary and not what must be used because of pellet mechanical issues);

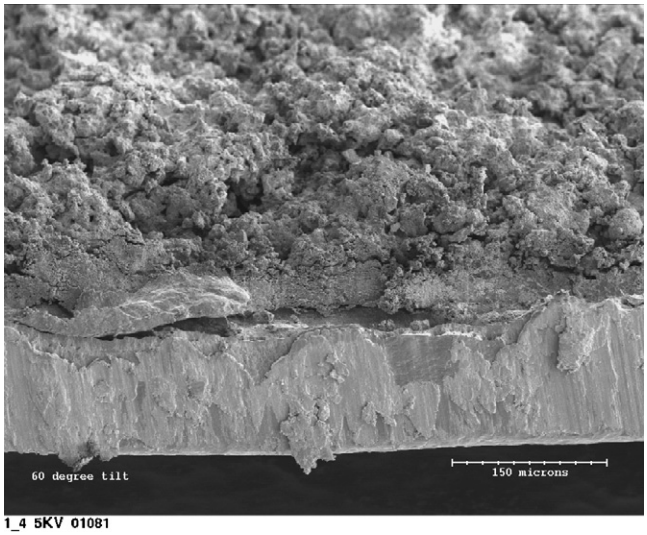

Fig. 15. Scanning electron microphotograph of plasma-sprayed pyrite cathode co-sprayed with LiCl–LiBr–LiF electrolyte. (Bottom layer is graphite-paper current collector.)

- reduction of the ohmic losses in the cathode because of better particle–particle contact;
- better wetting behavior of the cathode particles by the electrolyte;
- better contact (bonding) with the current collector;
- no need for expensive dies; inexpensive "cookie cutter" dies can punch any size and shape from a painted-cathode sheet.

However the thermal-sprayed cathode process presents several drawbacks:

- high cost of the process as the equipment is very expensive;
- loss of capacity for very thin electrodes due to self-discharge;
- the need to conduct the spraying under an inert atmosphere cover;
- presence of free sulfur when it is used as a thermal-barrier coating. This requires leaching of the sulfur from the electrode afterwards with CS_2. This issue was resolved by substitution of electrolyte as a barrier coating [156,146];
- a change in composition of the cathode from the starting feedstock material caused by large FeS_2 particle bouncing off the substrate, resulting in lower FeS_2 content;
- difficulty in controlling the density of the deposit. (The porous nature of the deposit is evident in Fig. 15.) A cross-sectional photomicrograph of a cell made with pressed-powder parts of nominal 25% porosity is shown in Fig. 16 (note the red color of the deposition band in the separator);
- it is a batch process, which makes it more difficult to commercialize.

Composite separator–cathode deposits were also prepared in the same manner by sequential thermal spraying of LiCl–KCl-based separator material onto a pyrite-cathode substrate [150,157]. Both single cells and batteries were tested using the two-layered, plasma-sprayed composites along with plasma-sprayed Li–Si anodes [158]. This was the first report of batteries made with all-plasma-sprayed electrodes.

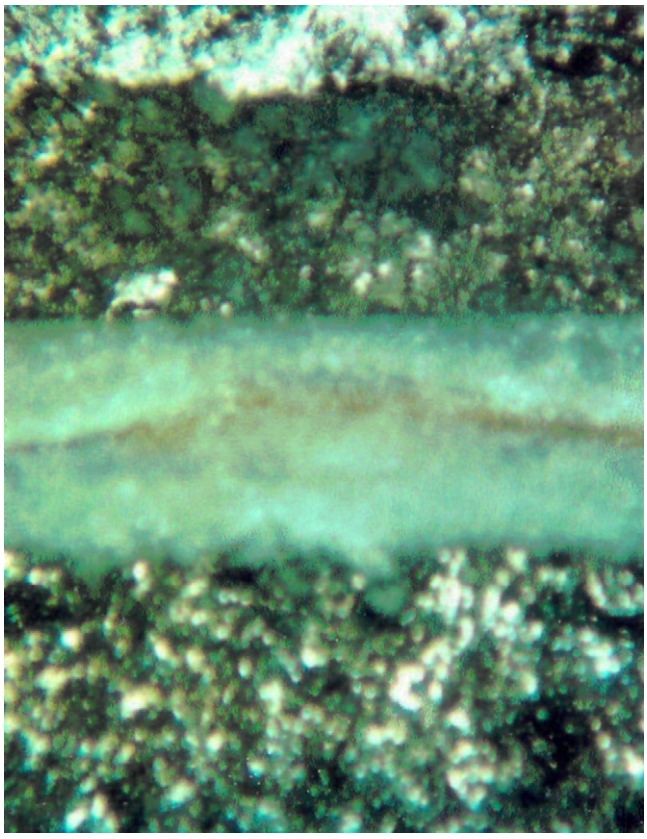

Fig. 16. Cross-sectional view of a Li–Si/LiCl–KCl/FeS_2 discharged cell. (The separator layer shows the colored deposition band noted earlier. The cathode is at the top of the picture; the separator layer is ~1 mm thick.)

More recently, work is underway studying the use of painted (sprayed) electrodes for thermal batteries [159]. This provides all of the advantages of plasma spraying without the disadvantages. Preliminary data for Li–Si/LiCl–KCl/FeS_2 cells made

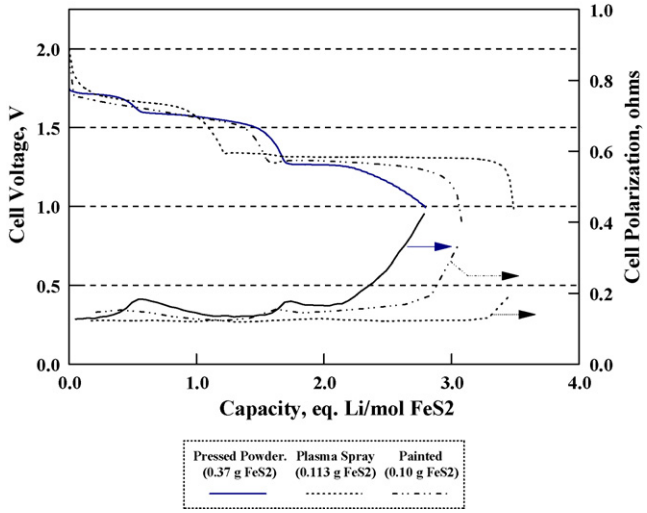

Fig. 17. Discharge at 500 °C and 125 mA cm^{-2} of cathode-limited, Li–Si (25% electrolyte)/LiCl–KCl/FeS_2 cells made with plasma-sprayed, painted, and pressed-powder cathodes.

with painted cathodes is presented in Fig. 17 along with comparable data for cells made with plasma-sprayed cathodes and pressed-powder cathodes. The lack of the large "humps" in the polarization traces for the cells with the sprayed and painted electrodes for the cathode voltage transitions is attributed to better particle–particle contact. Work is continuing to extend this approach to include the separator and anode, as well, with the goal of producing a three-layered, composite—a complete cell. This will greatly reduce the number of piece parts needed for battery assembly and will reduce the production costs of thermal batteries, if successful.

4. Conclusions

In this paper, we have presented an overview of the use of pyrite (FeS_2) as a cathode material for use in thermal batteries. The physical and chemical properties and the discharge sequences and reaction mechanisms are described including self-discharge processes.

References

[1] R.A. Guidotti, P. Masset, J. Power Sources 161 (2) (2006) 1443.
[2] P. Masset, R.A. Guidotti, J. Power Sources 164 (1) (2006) 397.
[3] A.A. Schneider, G.C. Bowser, US Patent 4,119,769 (October 10, 1978).
[4] Z. Tomzcuk, B. Tani, N.C. Otto, M.F. Roche, D.R. Vissers, J. Electrochem. Soc. 129 (5) (1982) 925.
[5] R.C. Sharma, Y.A. Chan, Metall. Trans. B 10B (1979) 103.
[6] W. Burgmann, G. Urbain, M.G. Frohberg, Mem. Sci. Rev. Metall. 65 (7–8) (1968) 567.
[7] P. Waldner, A.D. Pelton, Metall. Mater. Trans. B, Process Metall. Mater. Process. Sci. 35 (5) (2004) 897.
[8] S. Fiechter, M. Birkholz, A. Hartmann, P. Dulski, M. Giersig, T. Tributsch, R.J.D. Tilley, J. Mater. Res. 7 (7) (1992) 1829.
[9] J.A. Tossell, D.J. Vaughan, J.K. Burdett, Phys. Chem. Miner. 7 (1981) 177.
[10] G.L. Zhao, J. Callaway, M. Hayashibara, Phys. Rev. B 48 (21) (1994) 48.
[11] S.L. Finklea III, L. Cathey, E.L. Amma, Acta Crystallogr. A32 (1976) 529.
[12] J.A. Morice, L.V.C. Rees, D.T. Rickard, J. Inorg. Nucl. Chem. 31 (1969) 3797.
[13] L. Pauling, Can. Mineral. 16 (3) (1978) 447.
[14] A. Ennaoui, S. Fiechter, W. Jaergermann, H. Tribusch, J. Electrochem. Soc. 133 (1) (1986) 97.
[15] A. Sasaki, Mineral. J. 1 (5) (1955) 290.
[16] K.K. Mishra, K. Osseo-Asare, J. Electrochem. Soc. 135 (10) (1988) 2502.
[17] S.B. Lalvani, A. Weston, J.T. Masden, J. Mater. Sci. 25 (1A) (1990) 107.
[18] H.D. Banerjee, N. Godhaunkar, Mater. Lett. 10 (3) (1990) 99.
[19] J.C. Marinace, Phys. Rev. 96 (1954) 593.
[20] R. Otsuka, Synopsis, Graduate School of Science and Engineering, Waseda University, Japan, 1957, p. 6.
[21] S.L. Finklea, L. Cathey, Acta Crystallogr. A32 (1976) 529.
[22] V.P. Gupta, N.M. Ravindra, V.K. Srivastava, J. Phys. Chem. Solids 41 (1980) 145.
[23] T.A. Bither, Inorg. Chem. 7 (1968).
[24] H. Horita, T. Suzuki, Sci. Rep., Tohoku Univ. A-25 (4–5) (1975) 124.
[25] R. Schieck, A. Hartmann, S. Fiechter, R. Konenkamp, H. Wetzel, Mater. Res. 5 (7) (1990) 1567.
[26] O. Kubaschewski, C.B. Alcock, P.J. Spencer, Materials Thermochemistry, sixth ed., Pergamon Press, 1997.
[27] S.C. Mraw, D.F. Naas, J. Chem. Thermodyn. 11 (1979) 567.
[28] F. Gronvold, E.F. Westrum Jr., J. Inorg. Chem. 1 (1961) 36.
[29] F. Gronvold, E.F. Westrum Jr., J. Chem. Thermodyn. 8 (1976) 1039.
[30] P. Masset, Doctoral Thesis, National Polytechnic Institute of Grenoble, 2002.
[31] F.W. Dickson, L.D. Shields, G.C. Kennedy, Econ. Geol. 57 (7) (1962) 1021.
[32] E.T. Allen, R.H. Lombard, Am. J. Sci. 43 (255) (1917) 173.
[33] M.G. Reader, Kgl. Norske Videnskabers Selskab 2 (43) (1929) 151.
[34] F. de Rudder, Bull. Soc. Chim. Fr. 47 (1936) 1225.
[35] P. Toulmin III, P.B. Barton Jr., Geochim. Cosmochim. Acta 28 (1964) 641.
[36] S. Bog, T. Rosenqvist, Trans. Faraday Soc. 55 (1959) 1555.
[37] Y. Hong, B. Fegley Jr., Ber. Bunsenges. Phys. Chem. 101 (12) (1997) 1870.
[38] E.P. Schneeberg, Econ. Geol. 68 (1973) 507.
[39] H. Rau, J. Phys. Chem. Solids 37 (1976) 425.
[40] D'Or, J. Chim. Phys. 28 (1931) 378.
[41] B.J. Giletti, R.A. Yund, T.H. Lin, Econ. Geol. 57 (1968) 702.
[42] D. Ferro, V. Piacente, P. Scardala, J. Chem. Thermodyn. 21 (1989) 483.
[43] C.J. Johnson, J.L. Kavandi, Proc. ISE (Abstract 102) (1992) 145.
[44] J.E. Pahlman, G.W. Reimers, US Bureau of Mine Report RI9059 (1986).
[45] A.N. Spektor, A.D. Markov, A.N. Pyrikov, F.S. Umanskii, Zh. Prikladnoi Kh. 45 (8) (1972) 1713.
[46] J.P. Pemsler, R.K.F. Lam, J.K. Litchfield, S. Dallek, B.F. Larrick, B.C. Beard, J. Electrochem. Soc. 137 (1) (1990) 1.
[47] P.S. Thomas, D. Hirschauen, R.E. White, J.P. Guerbois, A.S. Ray, J. Therm. Anal. Cal. 72 (2003) 769.
[48] P. Masset, J.-Y. Poinso, J.-C. Poignet, J. Therm. Anal. Cal. 83 (2) (2006) 457.
[49] R.A. Guidotti, US Patent 4,731,307 (March 15, 1988).
[50] T.L. Aselage, E.E. Hellstrom, J. Electrochem. Soc. 134 (8) (1987) 1932.
[51] R.A. Guidotti, F.W. Reinhardt, W.F. Hammetter, Sandia Report SAND85-1737 (1988).
[52] R.A. Guidotti, F.W. Reinhardt, Proceedings of the 2nd Annual Battery Conference on Applications and Advances, 1987, p. 229.
[53] K. Grjotheim, B. Haugsdal, H. Kvande, H.G. Nebell, T.A. Utigard, J. Electrochem. Soc. 135 (1) (1988) 51.
[54] R.A. Guidotti, F.W. Reinhardt, Sandia Report SAND92-0874 (1992).
[55] V.S. Udintseva, G.I. Chuforov, J. Appl. Chem. USSR 14 (1941) 3.
[56] V.M. Zhukovskii, I.A. Montillo, A.A. Babadzhan, Tr. Ural. Nauch. Issled. Proek. Inst. Med. Prom. 8 (1967) 387.
[57] G.I. Samal, Geterogennye Khim. Reaktsii, Inst. Obshch. I Neorgan. Khim. Akad. Nauk Belorussk. SSR (1965) 93.
[58] G.M. Schwab, J. Philinis, J. Am. Chem. Soc. 69 (1947) 2588.
[59] B. Fegley Jr., K. Lodders, A.H. Treiman, G. Kleingelhofer, Icarus 115 (1995) 159.
[60] A.W. Coats, N.F.H. Bright, Can. J. Chem. 44 (1966) 1191.
[61] I.C. Hoare, H.J. Hurst, W.I. Stuart, T.J. White, J. Chem. Soc. Faraday Trans. 1 (84(9)) (1988) 3071.
[62] G. Pannetier, L. Davignon, Bull. Soc. Chim. 72 (1961) 1513.
[63] J.L.F. Monteiro, Can. J. Chem. Eng. 59 (1981) 511.
[64] S. Yamazaki, Z. Asaki, Y. Kondo, Trans. TMS-AIME 242 (1968) 896.
[65] M.D. Gibbs, T.N. Smith, B. Verbaan, Trans. Inst. Min. Metall. Section C 106 (1997) 69.
[66] M.D. Gibbs, T.N. Smith, B. Verbaan, Trans. Inst. Min. Metall. Section C 106 (1997) 74.
[67] A.G. Ritchie, P. Carter, Proceedings of the 38th Power Sources Conference, 1998, p. 215.
[68] P. Masset, V. Frotté, J.-Y. Poinso, J.-C. Poignet, J. Power Sources, to be submitted.
[69] S. Dallek, B.F. Larrick, Thermochim. Acta 95 (1985) 139.
[70] M.C. Hash, J.A. Smaga, R.A. Guidotti, F.W. Reinhardt, Proceedings of the 8th International Symposium on Molten Salts, 1992, p. 228.
[71] R.A. Sharma, R.N. Seefurth, J. Electrochem. Soc. 131 (5) (1984) 1084.
[72] C.H. Liu, A.J. Zielen, D.M. Gruen, J. Electrochem. Soc. 120 (1) (1973) 14.
[73] J. Phillips, H.F. Gibbard, Proceedings of the Second International Symposium on Molten Salts, The Electrochemical Society, Pennington, NJ, 81-10, p. 45.

[74] D. Warin, Z. Tomczuk, D.R. Vissers, J. Electrochem. Soc. 130 (1) (1983) 64.
[75] S. Sharma, J. Electrochem. Soc. 133 (5) (1986) 859.
[76] M.L. Saboungi, J.J. Marr, M. Blander, J. Electrochem. Soc. 125 (10) (1978) 1567.
[77] M.L. Saboungi, J.J. Marr, M. Blander, Metall. Trans. 10B (1979) 477.
[78] G. Santarini, Electrochim. Acta 27 (4) (1982) 495.
[79] Z. Tomczuk, S.K. Preto, M.F. Roche, J. Electrochem. Soc. 128 (4) (1981) 760.
[80] F.C. Mrazek, J.E. Battles, J. Electrochem. Soc. 124 (10) (1977) 1556.
[81] B. Tani, F. Mrazek, J. Faber, R. Hitterman, J. Electrochem. Soc. 133 (12) (1986) 2644.
[82] F.G. Bodewig, J.A. PLambeck, J. Electrochem. Soc. 117 (7) (1970) 904.
[83] D.M. Gruen, R.L. McBeth, A.J. Zielen, J. Am. Ceram. Soc. 93 (24) (1971) 6691.
[84] G. Delarue, Bull. Soc. Chim. Fr. (1969) 906.
[85] G. Delarue, J. Electroanal. Chem. 1 (1959) 43.
[86] G. Delarue, J. Electroanal. Chem. 1 (1960) 285.
[87] G. Delarue, Bull. Soc. Chim. Fr. (1960) 1654.
[88] G. Barlow, Investigation of Mechanism for Capacity Loss in Iron Disulfide Electrodes in High-Temperature Lithium-Alloy/Metal Sulfide Batteries, Final Report to Lawrence Berkeley Laboratory, December 1986.
[89] P. Masset, J.-Y. Poinso, S. Schoeffert, J.-C. Poignet, Proceedings of the 39th International Power Sources Conference, 2002, p. 246.
[90] P. Masset, Z. Naturforsch., in press.
[91] T.L. Aselage, E.E. Hellstrom, J. Electrochem. Soc. 134 (8) (1987) 1929.
[92] R.A. Guidotti, F.W. Reinhardt, J. Odinek, J. Power Sources 136 (2) (2004) 257.
[93] R.A. Guidotti, R.A. Normann, F.W. Reinhardt, J. Odinek, Trans. Geothermal Resour. Council 27 (2003) 173.
[94] R.A. Guidotti, F.W. Reinhardt, Proceedings of The Electrochemical Society, vol. 2002-19 (Molten Salts XIII), 2002, p. 63.
[95] R.A. Guidotti, Proceedings of the 35th IECEC Meeting, vol. 2, 2000, p. 1276.
[96] R.A. Guidotti, F.W. Reinhardt, Proceedings of the International Symposium on Molten Salts, XII, vol. 99-41, 2000, p. 701.
[97] R.A. Guidotti, F.W. Reinhardt, Proceedings of the 11th International Symposium on Molten Salts, 1998, p. 316.
[98] R.A. Guidotti, F.W. Reinhardt, Proceedings of the 41st Power Sources Conference, 2005, p. 141.
[99] R.A. Guidotti, F.W. Reinhardt, Proceeding of 201st ECS Meeting, Molten Salts, XIII, PV 2002-19, The Electrochemical Society, Pennington, NJ, 2002, p. 31.
[100] E. Strauss, D. Golodnitsky, E. Peled, Electrochim. Acta 45 (2000) 1519.
[101] E. Strauss, D. Golodnitsky, E. Peled, Electrochem. Solid State Lett. 2 (3) (1999) 115.
[102] D. Golodnitsky, E. Peled, Electrochim. Acta 45 (1999) 335.
[103] E. Peled, D. Golodnitsky, E. Strauss, J. Lang, Y. Lavi, Electrochim. Acta 43 (10–11) (1998) 1593.
[104] E. Peled, D. Golodnitsky, J. Lang, Y. Lavi, in: N. Doddapaneni, A.R. Landgrebe (Eds.), Proceeding of the Symposium on Lithium Batteries, PV 94-4, The Electrochemical Society, Pennington, NJ, 1994, p. 75.
[105] C. Iwakura, N. Isobe, H. Tamura, Electrochim. Acta 28 (3) (1983) 277.
[106] Y. Shao-Horn, Q.C. Horn, Electrochim. Acta 46 (2001) 2613.
[107] Y. Shao-Horn, S. Osmialowski, Q.C. Horn, J. Electrochem. Soc. 149 (11) (2002) A1499.
[108] J.-W. Choi, G. Cheruvally, H.-J. Ahn, K.-W. Kim, J.-H. Ahn, J. Power Sources 163 (1) (2006) 158.
[109] Y. Shao-Horn, S. Osmialowski, Q.C. Horn, J. Electrochem. Soc. 149 (12) A1547.
[110] T.D.J. Dunstan, J. Caja, R.A. Guidotti, in: P.C. Truelove, H.C. Delong, R.A. Mantz, G.R. Stafford, M. Matsunaga (Eds.), Proceeding of the International Symposium on Molten Salts XIII, vol. 2002-19, 2002, p. 43.
[111] R.A. Guidotti, S. Preston, D. Pickett, Z. Johnson, J. Wilkes, Proceedings of the 42nd Power Sources Conference, 2006, p. 241.
[112] K. Abe, T. Chiku, J. Electrochem. Soc. 122 (10) (1975) 1322.
[113] S.S. Wang, R.N. Seefurth, J. Electrochem. Soc. 134 (3) (1987) 530.
[114] J.A. Schmidt, An. Asoc. Quim. Argent. 74 (2) (1986) 149.
[115] J.A. Schmidt, An. Asoc. Quim. Argent. 75 (3) (1987) 359.
[116] Z. Tomczuk, D.R. Vissers, J. Electrochem. Soc. 133 (12) (1986) 2505.
[117] S.K. Preto, Z. Tomczuk, S. von Winbush, M.F. Roche, J. Electrochem. Soc. 130 (2) (1983) 264.
[118] D. Guerard, A. Herold, Carbon 3 (4) (1975) 337.
[119] M. Armand, University of Grenoble, 1978 (in French).
[120] A. Ritchie, Proceedings of the 18th International Power Sources Symposium, 1993, p. 299.
[121] D.M. Chen, H.F. Gibbard, J. Electrochem. Soc. 130 (10) (1983) 1975.
[122] L. Redey, J.A. Smaga, J.E. Battles, R. Guidotti, Argonne National Laboratory Report ANL-87-6 (1987).
[123] S.P.S. Badwal, R.J. Thorn, J. Sol. St. Chem. 43 (1982) 163.
[124] R.A. Guidotti, unpublished data.
[125] L. Redey, D.R. Vissers, J. Electrochem. Soc. 128 (12) (1981) 2703.
[126] Z. Tomczuk, L. Redey, D.R. Vissers, J. Electrochem. Soc. 130 (5) (1983) 1074.
[127] L. Redey, D.R. Vissers, J. Electrochem. Soc. 130 (1) (1983) 231.
[128] S.S. Wang, J. Electrochem. Soc. 135 (7) (1988) 1675.
[129] R. Fong, J.R. Dahn, C.H.W. Jones, J. Electrochem. Soc. 136 (11) (1989) 3206.
[130] F. Fong, C.H.W. Jones, J.R. Dahn, J. Power Sources 26 (3–4) (1989) 333.
[131] R.A. Guidotti, F.W. Reinhardt, J.A. Smaga, Proceeding of the 34th International Power Sources Symposium, 1990, p. 132.
[132] L. Redey, Argonne National Laboratory, unpublished data.
[133] B.J. Burrow, K.W. Nebesny, N.R. Armstrong, R.K. Quinn, D.E. Zurawski, J. Electrochem. Soc. 128 (9) (1981) 1919.
[134] Argonne National Laboratory Progress Report for October 1980–September 1981, ANL-81-65 (1981).
[135] N. Takami, N. Koura, Proceedings of the Stationary Energy Storage Load Leveling and Remote Applications, PV 88-11, The Electrochemical Society, 1988, p. 106.
[136] M.J. Weaver, D. Inman, Electrochim. Acta 20 (1975) 929.
[137] Z. Tomzcuk, D.R. Vissers, J.L. Saboungi, Proceedings of the Fourth International Symposium on Molten Salts, PV 84-2, The Electrochemical Society, 1984, p. 352.
[138] J.J. Warren Jr., in: G. Mamamtov, R. Marassi (Eds.), Molten Salts Chemistry, 1987, p. 237.
[139] A.S. Dworkin, H.R. Bronstein, M.A. Bredig, J. Phys. Chem. 66 (1962) 572.
[140] R. Knödler, J. Electrochem. Soc. 130 (1) (1983) 16.
[141] G.M. Haarberg, K.S. Osen, J.J. Heus, J.J. Egan, J. Electrochem. Soc. 137 (9) (1991) 2777.
[142] G.M. Haarberg, K.S. Osen, J.J. Egan, H. Heyer, W. Freyland, Ber. Bunsenges. Phys. Chem. 92 (1988) 139.
[143] G.J. Reynolds, M.C.Y. Lee, R.A. Huggins, Proceedings of the Fourth International Symposium on Molten Salts, PV 84-2, The Electrochemical Society, 1984, p. 579.
[144] M. Au, J. Power Sources 115 (2) (2003) 360.
[145] R.A. Guidotti, P.J. Nigrey, F.W. Reinhardt, J.G. S Odinek, Batteries Proceeding of the 40th Power Sources Conference, 2002, p. 250.
[146] R.A. Guidotti, H. Ye, T.D. Xiao, D.E. Reisner, D.H. Doughty, US Patent 6,926,997 (August 9, 2005).
[147] R.A. Guidotti, F.W. Reinhardt, J. Dai, J. Roth, D.E. Reisner, Proceedings of the 41st Power Sources Conference, 2004, p. 153.
[148] J. Dai, R.A. Guidotti, T.D. Xiao, D.E. Reisner, US Patent 6,794,086 (September 21, 2004).
[149] R.A. Guidotti, F.W. Reinhardt, J. Dai, T.D. Xiao, D. Reisner, Proceedings of the 35th IECEC Meeting, vol. 2, 2002, p. 976.
[150] R.A. Guidotti, F.W. Reinhardt, J. Dai, D.E. Reisner, Proceedings of the 40th Power Sources Conference, 2002, p. 339.
[151] R.A. Guidotti, F.W. Reinhardt, J. Dai, D.E. Reisner, Proceedings of the 36th IECEC, vol. 1, 2001, p. 897.
[152] R.A. Guidotti, F.W. Reinhardt, J. Dai, T.D. Xiao, D.E. Reisner, Review of US Nanocorp®—SNL Joint Development of Thermal-Sprayed Thin-Film Cathodes for Thermal Batteries, 16th Annual Conference on Applications and Advances, Long Beach, CA, January 9–12, 2001.

[153] J. Broadhead, J. Dai, J. Roth, R.A. Guidotti, D. Reisner, Thermal-Sprayed Thin-Film Electrodes for Primary and Secondary Batteries, IBA-2001 Battery Materials Symposium, Pilanesberg, S. Africa, March 11–14, 2001.
[154] R.A. Guidotti, F.W. Reinhardt, J. Dai, J. Roth, D.E. Reisner, Proceedings of the 17th Conference on Applications and Advances, 2001, p. 97.
[155] R.A. Guidotti, J. Dai, T.D. Xiao, D.E. Reisner, Proceedings of the 15th Annual Conference on Applications and Advances, 2000, p. 127.
[156] D.E. Reisner, T.D. Xiao, J. Dai, R.A. Guidotti, F.W. Reinhardt, J. New Mater. Electrochem. Syst. 2 (1999) 279.
[157] R.A. Guidotti, F.W. Reinhardt, J. Dai, D.E. Reisner, J. Power Sources 160 (2) (2006) 1456.
[158] C.J. Crowley, N.A. Elkouth, C. Lamb, Proceedings of the 39th Power Sources Conference, 2000, p. 517.
[159] Work underway at Electro Energy, Inc., Colorado Springs, CO, under US Navy SBIR Phase II program.
[160] P.J. Masset, R.A. Guidotti, J. Power Sources (2007), doi:10.1016/j.jpowsour.2007.11.073.